


# A Lower Limb-Pelvis Finite Element Model with 3D Active Muscles

FUHAO MO <sup>1</sup>, FAN LI,<sup>1</sup> MICHEL BEHR,<sup>2</sup> ZHI XIAO,<sup>1</sup> GUANJUN ZHANG,<sup>1</sup> and XIANPING DU<sup>3</sup>

<sup>1</sup>State Key Laboratory of Advanced Design and Manufacture for Vehicle Body, Hunan University, Changsha, Hunan 410082, China; <sup>2</sup>Laboratoire de Biomécanique Appliquée (IFSTTAR - Université de la Méditerranée), Faculté de Médecine Nord, Boulevard Pierre Dramard, 13916 Marseille Cedex 20, France; and <sup>3</sup>Department of Mechanical Engineering, Embry-Riddle Aeronautical University, Daytona Beach, FL 32114, USA

(Received 28 June 2017; accepted 7 October 2017; published online 16 October 2017)

Associate Editor Eiji Tanaka oversaw the review of this article.

**Abstract**—A lower limb-pelvis finite element (FE) model with active three-dimensional (3D) muscles was developed in this study for biomechanical analysis of human body. The model geometry was mainly reconstructed from a male volunteer close to the anthropometry of a 50th percentile Chinese male. Tissue materials and structural features were established based on the literature and new implemented experimental tests. In particular, the muscle was modeled with a combination of truss and hexahedral elements to define its passive and active properties as well as to follow the detailed anatomy structure. Both passive and active properties of the model were validated against the experiments of Post-Mortem Human Surrogate (PMHS) and volunteers, respectively. The model was then used to simulate driver's emergency braking during frontal crashes and investigate Knee-Thigh-Hip (KTH) injury mechanisms and tolerances of the human body. A significant force and bending moment variance was noted for the driver's femur due to the effects of active muscle forces during emergency braking. In summary, the present lower limb-pelvis model can be applied in various research fields to support expensive and complex physical tests or corresponding device design.

**Keywords**—Muscle, Lower limb, Pelvis, Active contraction, Finite element analysis.

## INTRODUCTION

The lower limb injury is one of the most common injury types suffered from traffic accidents or sport activities. Numerical human model is a very useful tool to understand joint kinematics and injury mechanisms of human body under various loading conditions, and improve relevant protection or assistant device design.

Among them, the musculoskeletal model is easy to simulate joint kinematics but hard to monitor stress distribution of anatomy structures. However, this can be easily achieved by finite element simulations. Many lower limb FE models were developed from early simplified rigid bone and hinge-like joint model to latest active muscle FE models in previous decades, in order to in-depth investigate human lower limb injury mechanisms especially in traffic accidents. Several FE models included detailed anatomy structures and a series of validation works against Post-Mortem Human Surrogate (PMHS) tests. But most of them still only include passive muscle properties without active contraction like *in vivo* skeletal muscle, or some consist of simplified 1D muscle elements without detailed anatomy geometry.

Beillas *et al.*<sup>6</sup> built the Lower Limb Model for Safety (LLMS) with about 25,000 elements on the basis of computed tomography (CT) and magnetic resonance imaging (MRI) scans of a 50% European male. Then it was continuously improved and further validated by sequent studies according to new modelling methods or implemented experimental tests.<sup>3,5,23</sup> The cortical bone of long shafts and epiphyses were both modelled in shell elements with different thickness. Takahshi *et al.*<sup>31</sup> developed a pedestrian lower limb FE model in PAM-CRASH codes based on volunteer MRI data, then which was combined with a pelvis model developed by Kikuchi *et al.*<sup>19</sup> based on a 50% male CT data. Iwamoto *et al.*<sup>14</sup> established an occupant lower limb model based on the geometries reconstructed from the Viewpoint Datalabs™ dataset. On the basis of this model, an entire human body model—the THUMS model was developed. Subsequently, the THUMS model was continuously improved till version 4.0.<sup>29,36</sup> Untaroiu *et al.*<sup>33</sup> developed

---

Address correspondence to Fuhao Mo, State Key Laboratory of Advanced Design and Manufacture for Vehicle Body, Hunan University, Changsha, Hunan 410082, China. Electronic mail: fuhao@hnu.edu.cn

a pedestrian lower limb FE model without below ankle part in LS-Dyna codes using Visible Human Male Project/CT technology. Then an occupant lower limb FE model was built based on the method and materials used in above-mentioned pedestrian lower limb model,<sup>35</sup> which was validated against latest published experimental results.<sup>13,34</sup> And Shin *et al.*<sup>30</sup> also present an ankle and foot region model that will be coupled with the above-mentioned lower limb model to create a state-of-art human model for automotive safety. As indicated by the Untaroiu *et al.* study,<sup>35</sup> the main limitations of existing lower limb FE models comes from their geometries, the modeling approaches employed to represent their components, and limited test data available for model validation at the time when the models were developed. In addition, most models defined muscle as several simple blocks to resist compression and impact, and physical active contraction was usually modelled with 1D type elements that attached on muscle insertions directly. Few models defined muscle blocks according to detailed anatomy structures, less was of active 3D muscles.

This study aims to develop a biofidelic lower limb-pelvis FE model with detailed active 3D muscle groups, and validate the model availability not only against PMHS tests but also volunteer motion tests. The model geometry was reconstructed from CT and MRI scan data of a 50th percentile Chinese male volunteer. The muscles were modelled with a combination of 3D solids and 1D truss elements following anatomy blocks to represent passive and active properties, respectively. Their material properties were rigorously determined based on the appropriate literature data with strain rate effects in consideration. The components of the lower limb model and the model entirety were validated against the latest PMHS test data and volunteer gait data. Finally, the present model was used to analyze driver's KTH injury mechanisms under active muscle forces during emergency braking.

## METHODS AND MATERIALS

### *Development of a Lower Limb-Pelvis FE Model with Active 3D Muscles*

#### *Geometry Reconstruction*

This study was approved by the Second Xiangya Hospital committee for clinical research (NO. 2012-S231) and informed consent were obtained from the volunteers. The geometry reconstruction of the model was based on a volunteer (173.1 cm height and 69.7 kg weight) with an anthropometry close to the 50th percentile male. The geometry of bony structures was mainly extracted from the computed tomography (CT)

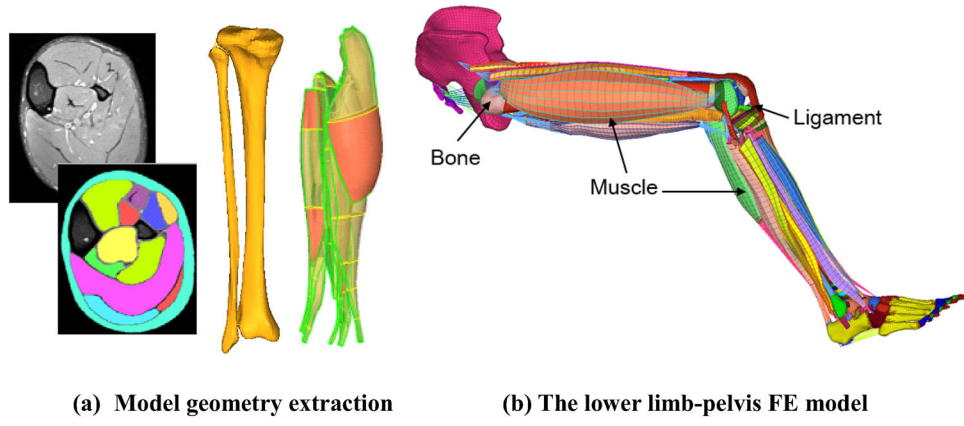
scans. Soft tissue structures were mainly reconstructed on the basis of the MRI scans with the axial interval at 4.1 mm, and 0.33–0.34 mm intervals in both sagittal and coronal plane.

Medical engineering software Mimics was used to extract the model geometry and followed by geometric processing with the Geomagic software. As the muscle groups present complex geometry, the entity mapping function of HyperMesh was used to partition their geometry structures by repeatedly cutting the geometry, defining the source plane, and finally mapping the hexahedral elements based on the defined geometry (Fig. 1a). The whole model consists of 355,847 elements with 22 muscle groups as shown in Fig. 1b, of which there are 242,011 solid elements, 87,533 shell elements, 23,793 active contraction truss elements and 1116 spring elements. The total weight of a single limb model is 7.874 kg.

#### *3D Active Muscle Modeling*

The present lower limb-pelvis model was developed in LS-DYNA codes. As shown in Fig. 2, the FE model of each muscle consists of three parts, namely the tendon unit (TU), muscle passive unit (PU) and active contraction unit (CU). The muscle force is composed of passive elongation or compression force of the PU element, active contraction force of the CU element and tendon elongation force of the TU element. The tendon was modelled with 1D nonlinear spring element in series. The middle muscle was represented by a combination of 3D hexagonal elements and surrounding 1D truss elements, which corresponds exactly to the anatomical characteristics of skeletal muscles. The truss elements were generated surrounding 3D hexagonal elements automatically by Matlab codes along the muscle fiber direction. The 1D truss elements represented muscle active contraction unit namely the muscle fibers related to the contractile protein of myofibrillar, actin and myosin. The 3D hexagonal elements represented the muscle passive unit related to the connective tissues around the muscle fibers like the outer membrane, the muscle bundle membrane, the sarcolemma and so on. The starting and ending points have a great influence on the force direction and torque of the total muscle. All the lower limb muscle insertions referred exactly to the points of muscle anatomical attachments.

Passive properties of the muscle modelled through 3D hexagonal elements was given by the hyperelastic material (Ogden constitutive model) with strain rate effects. As shown in Table 1, the material parameters were acquired on the basis of the experimental test data from Myers *et al.* studies.<sup>24,25</sup> Although the skeletal muscle was anisotropic, the present model



(a) Model geometry extraction

(b) The lower limb-pelvis FE model

FIGURE 1. Development of a lower limb-pelvis FE model.

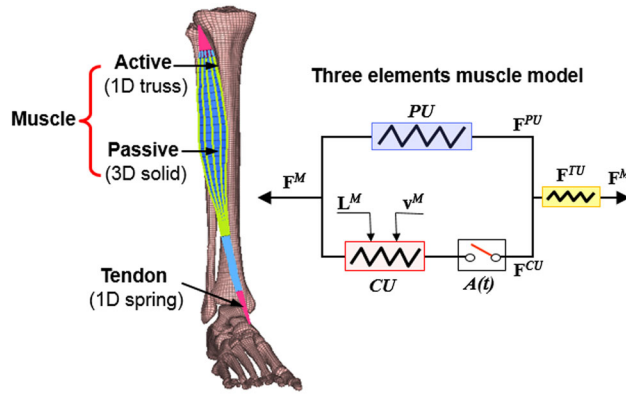


FIGURE 2. 3D muscle model by the combination of three elements.

assumed it as isotropic material in the consideration of computing stability and efficiency.

Active property of the muscle modelled by a series of truss elements was given by the Hill constitutive material model. The active contraction force produced by the muscle was determined as follows.

$$F^{CE} = A(t)F_1(l)F_v(v)F_{\max} \quad (1)$$

where  $A(t)$  is the muscle activation level,  $F_1(l)$  is the normalized force-length curve,  $F_v(v)$  is the force-velocity curve and  $F_{\max}$  is the maximum isometric force. The normalized force-length and force-velocity curves were produced by previous empirical expressions as follows.<sup>37-39</sup>

$$F_1(l) = \text{Exp}\{-[(l/l_{\text{opt}} - 1)/C_{\text{sh}}]^2\} \quad (2)$$

$$F_v(v) = \begin{cases} 0 & v_n \leq -1 \\ (1 + v_n)(1 - v_n/C_{\text{short}}) & -1 < v_n \leq 0 \\ [1 + v_n(C_{\text{mvl}}/C_{\text{leng}})]/(1 + v_n/C_{\text{leng}}) & 0 < v_n \end{cases} \quad (3)$$

TABLE 1. Muscle passive properties by the Ogden model.

Parameters	Ogden model (MAT 77)
Density	$\rho(\text{kg/m}^3) = 1.12$
Poission ratio	$\nu = 0.495$
Elastic responses	$\mu_1(\text{MPa}) = 0.01148$ $\alpha_1 = 12.32$
Visco responses	$G_A(\text{MPa}) = 0.001;0.575;0.288;0.137$ $\beta_i(\text{s}^{-1}) = 73.4;50.3;42.7;0.255$

Where  $l_{\text{opt}}$  is the length at which active muscle force peaks or optimal muscle fiber length, and  $C_{\text{sh}}$  is a dimensionless shape parameter;  $v_n$  is the normalized maximum muscle shortening velocity, and  $C_{\text{short}}$ ,  $C_{\text{leng}}$ ,  $C_{\text{mvl}}$  are shape parameters controlling the force-velocity curve. Some modeling details have been reported in the previous study.<sup>21</sup> The maximum isometric force was defined by the product of the PCSA (Physiological Cross Sectional Area) of each muscle and a normalized stress value 0.5 MPa.<sup>38,39</sup> The calculated maximum isometric force of all model muscles are shown in the Appendix Table 3.

### Bone and Other Tissues

Long bones were modeled following their anatomy structures such as bone shaft, proximal and distal epiphysis (Fig. 3). The cortical and spongy bone were divided into several regions considering the thickness and density variance recorded by the CT scan. The cortical bones located on the two ends were modeled using shell elements with different thickness. The cortical bone of the shaft region and the spongy bones were all represented with solid elements. At least three layers of hexahedral elements were used in the long bone shaft in order to consider convergence and precision of the calculation results.<sup>16</sup> ANSYS ICEM CFD modular was adopted for bone meshing by firstly generating block topology based on the bone geometry, then projecting the resulting parametric grids onto the defined geometry to obtain high quality hexahedral meshes.

In vehicle crash safety, most of the bone fractures are caused by the pressure load (62%), followed by the bending moment load (24%), and the torsional and shear loads only accounted for about 5% respectively.<sup>9</sup> For cortical bones, an isotropic elastic-plastic material (MAT 124) which defines the tensile and compressive properties was adopted. The strain rate effect was also included in the modeling of cortical bones and realized by scaling the compressive and tensile yield stress as follows.

$$\sigma_{yD} = \sigma_{y0} \left( 1 + \left( \frac{\dot{\epsilon}}{C} \right)^{1/p} \right) \quad (4)$$

Where  $\sigma_{yD}$  is scaled yield stress under dynamic loading with strain rate  $\dot{\epsilon}$ , and  $\sigma_{y0}$  is yield stress under statistic

loading;  $C$  and  $P$  are controlling parameters based on experimental data. As the spongy bone presents a porous structure which acts like a buffer under the impact loading, an elastic viscoplastic material model (Mat 105) combined with continuous damage mechanics (CDM) was selected for spongy bones. In this study, bone material constants, post yield material behavior and damage controlled by strain–stress curves were determined from previous studies.<sup>1,6,22,35</sup> Validation of bone structures under various loading environments have been reported in previous studies.<sup>8,9</sup> Material details supporting bone modeling are briefly listed in Table 2.

In addition, detailed anatomy structures were included in the joint part, such as the ligaments, joint capsules, cartilages and meniscus. The four main knee ligaments were modeled using quasi linear viscoelastic (QLV) material model referring to the previous modeling method.<sup>33</sup>

### Validation of the Active Lower Limb-Pelvis Model

#### Example of Passive Property Validation

The active lower limb-pelvis model has been validated in a series of experimental tests ranging from isolated tissue tests to the whole limb impacts. Some details to support modelling validation were presented in the previous studies.<sup>8,9,16</sup> Recent published experimental data were used for model validation and improvement. For examples, the long bone models with surrounding muscles were validated against dynamic three-point bending experiments of various directions and locations in recent studies.<sup>17,18</sup> Knee,

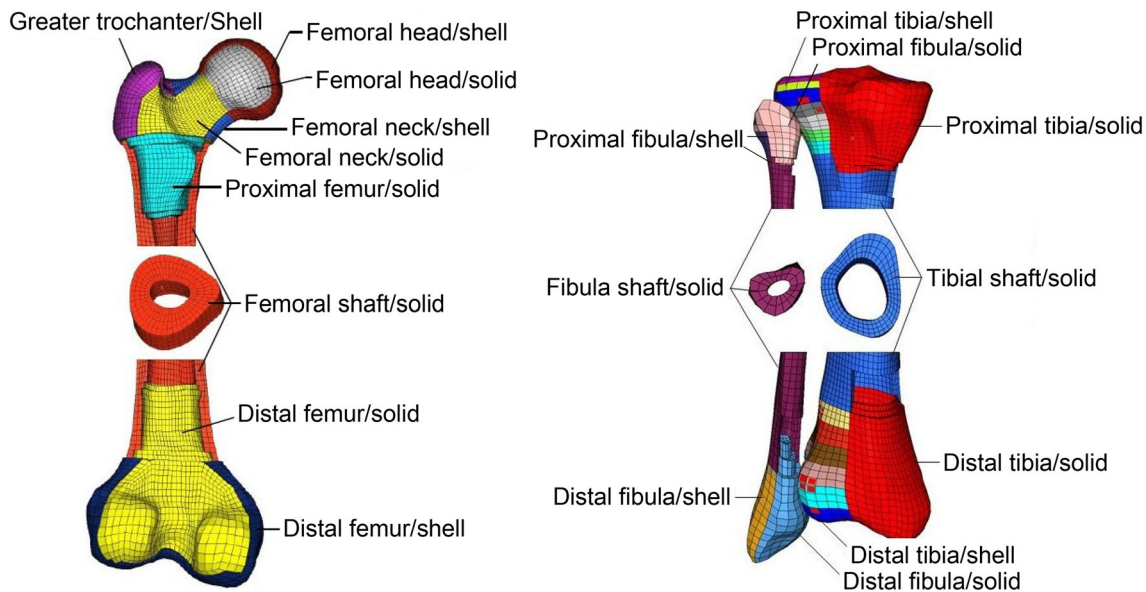
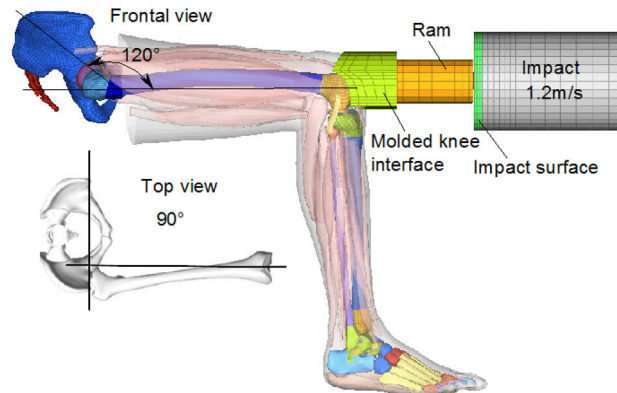


FIGURE 3. Long bone modelling based on detailed anatomy structures.



**TABLE 2. Summary of material properties of bones.**

	Density (g/mm <sup>3</sup> )	Young's modulus (MPa)	Poisson's ratio	Yield stress (MPa)	Ultimate strain
Cortical bones	0.0018–0.002	2000–20000	0.3	65–120	0.7–2.4%
Spongy bones	0.00086–0.0015	160–700	0.3–0.33	3.7–9.3	0.9–13.4%

**FIGURE 4. Knee impact simulation model.**

ankle and hip joints were validated against foot axial impact and knee impact tests.<sup>11,20,28</sup>

The implemented validation for the Knee-Thigh-Hip (KTH) segment with Rupp *et al.*<sup>28</sup> experimental data were shown in the present study (Fig. 4). Following the experimental procedure, the hip joint was set in neutral position, namely the connecting line between the femoral condyle center and the hip joint center is in horizontal. The knee flexion angle was set to 90°, while the hip flexion and abduction angles were set as 120° and 90°, respectively. As the pelvis muscles were removed, the clamping block was used to restrain pelvis iliac crest. The initial velocity of the impactor was set to 1.2 m/s. By the definition of 13 mm buffering cushion and rigid knee contour cushion, the increasing rate of the impact force at 300 N/ms was obtained as desired maximum loading rate in the experimental test.

Among 19 cases of the impact tests conducted by Rupp *et al.*,<sup>28</sup> except that one of them was without bone fracture, the fractures of all other cases were mainly distributed in the posterior wall of the acetabulum (10 cases), the acetabular T (2 cases), acetabular edge (3 cases), pubic branch (6 cases), iliac crest (1 case) and femoral neck (3 cases). The average tolerance of the KTHs in the experiments was  $5.7 \pm 1.88$  kN, and the statistical time was  $38.3 \pm 11.5$  ms after the shock. Comparing the experimental and simulation results (Fig. 5), the simulation result was in the experimental corridor with a load peak of 5.81 kN at 32.9 ms after the knee shock. The damage of the simulation case was located at the articular cartilage of the

acetabular posterior and acetabular edge. Therefore, the failure time, location and peak force of the simulation have a good correspondence with the experiments. It can be concluded that the whole model has good biological fidelity and can be used in the subsequent study of lower limb and pelvis injuries.

#### Example of Active Property Validation

To validate active properties of the lower limb-pelvis model, the gait analysis of swing phase from the maximum angle of 65° to the minimum angle of 0° was implemented using the present FE model. The total simulation time is 220 ms. Because the EMG signal of deep muscle groups cannot be detected in a volunteer gait test, the direct application of surface electrode EMG signal on the FE lower limb-pelvis model is not robust for gait analysis. Therefore, reverse kinetic optimization algorithm using a musculoskeletal model was implemented to obtain active levels of each muscle during a gait cycle. The validated musculoskeletal model in Opensim codes was used for the preliminary gait analysis.<sup>2</sup> By the input of volunteer kinematic parameters, the activation levels of each muscle were obtained by muscle controlling calculation. Four typical activation level curves of total 22 muscles were shown in Fig. 6. By comparing with EMG data from the experiments, the obtained muscle activation levels were evaluated and verified.<sup>26,32</sup>

The initial position of the lower limb-pelvis FE model was adjusted to 65° for the knee joint, and the hip joint was adjusted to the standing posture. The activation level obtained from the musculoskeletal

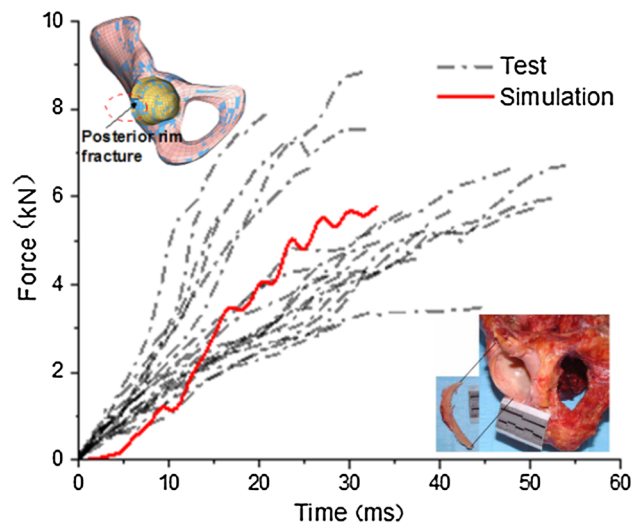


FIGURE 5. Comparison of the KTH impact simulation with experimental results.

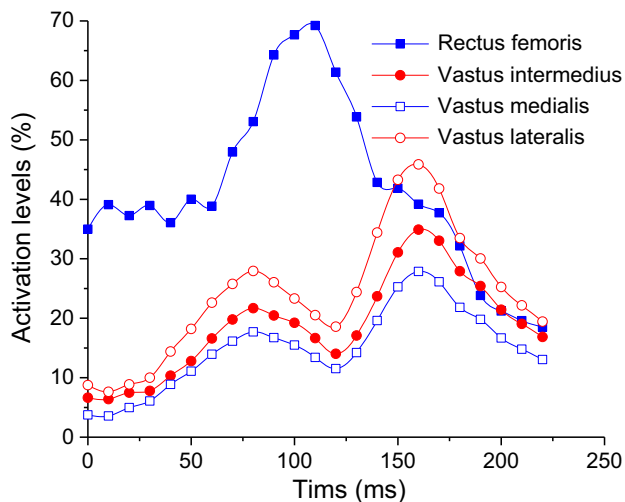


FIGURE 6. Typical muscle activation levels of the swing phase during gait analysis.

analysis were applied on 3D muscles of the lower limb-pelvis model. Muscle activation levels from the musculoskeletal analysis and active contractile force cloud image from the FE simulation were shown in Fig. 7.

In addition, the knee flexion angle of the FE model was extracted from the angle between tibial axis and femoral axis. The comparison of the gait test data<sup>2</sup> to the simulation results was shown in Fig. 8. In summary, activation level, contraction force and joint flexion angle are in a good correspondence during the whole knee extension process. The frontal muscles of thigh present largest contraction force while the frontal muscle forces of the lower leg increase the ankle dorsiflexion to stabilize the heel before loading.

#### *Application for Simulating Emergency Brake During Vehicle Frontal Impact*

Emergency braking tests were implemented in French IFSTTAR Laboratory of Applied Biomechanics. Eleven healthy male volunteers with driving experience more than 2 years (mean age:  $42 \pm 5$  years; age range: 22–67 years; mean weight:  $83 \pm 5$  kg) were explored. The volunteers were required to sit on a driving simulator with a constant force of 4 N on the accelerator pedal, and follow the red light signal to make an emergency brake (Fig. 9a). Braking force, braking time, electromyographic (EMG) activities and related joint kinematics were recorded in the experiments. The experimental details have been reported in the Yves *et al.* study.<sup>15</sup>

A FE simulation model of emergency braking was established according to the experimental test conditions (Fig. 9b). Muscle activation levels of the lower limb-pelvis model were based on the normalized EMG signals reported in the present tests or previous studies. The initial peak of the braking force was 725.1 N which appeared around 30.7 ms. The follow-up braking force remained around the experimental value of 759 ( $s = 74$ ) N with stable fluctuation. The medial gastrocnemius muscle and the tendon region in the posterior part of the calf show the largest active contractile force, which is basically consistent with the normal physiological activity of the volunteers. All these indicated the robustness of the lower limb-pelvis model and its availability for further research in crash safety.

To investigate the influences of active muscle force on occupant KTH injuries, 25% offset crash simulations with occupant emergency braking action and

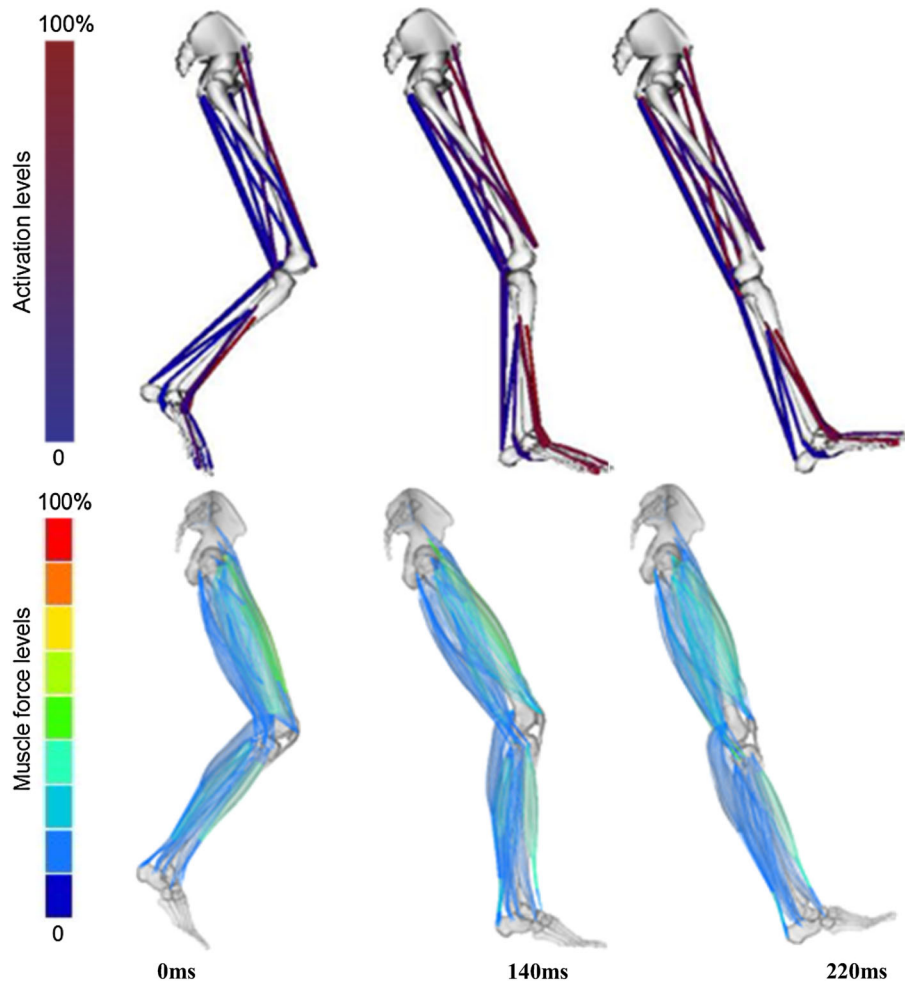


FIGURE 7. Comparison of joint kinematics between the musculoskeletal analysis and FE simulation.

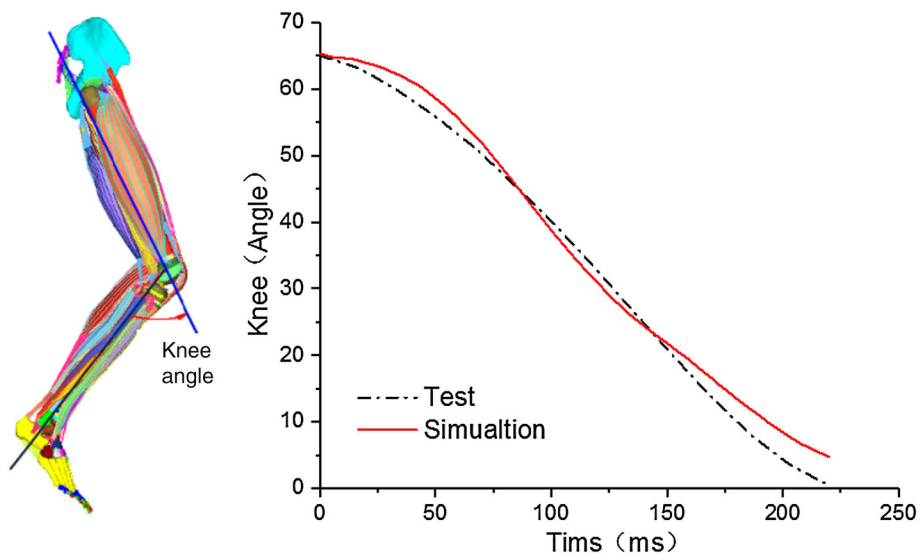


FIGURE 8. Comparison of knee joint angles from the FE simulation to the experimental data.

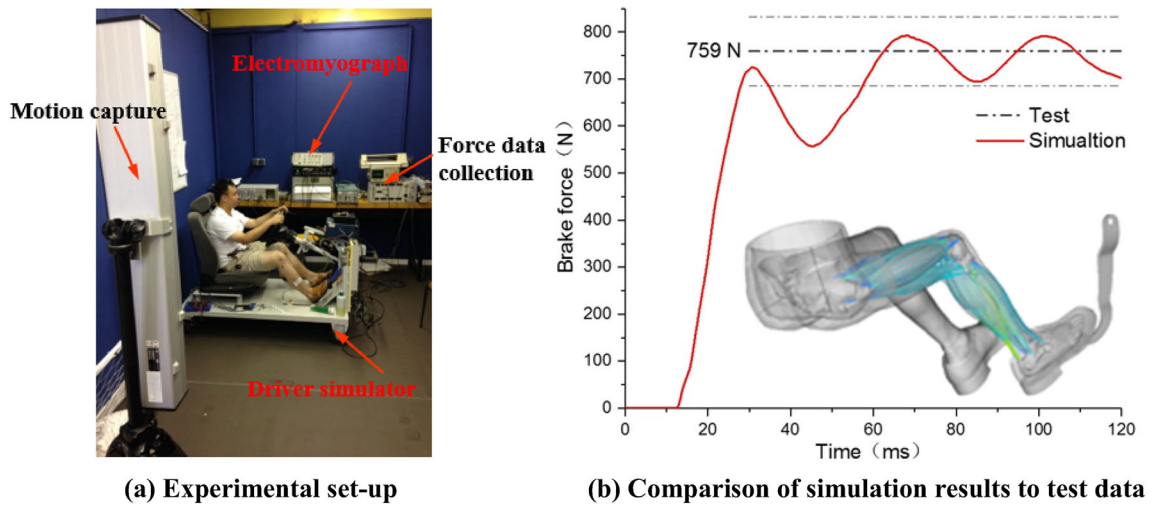


FIGURE 9. Experimental set-up and its comparison with the simulation.

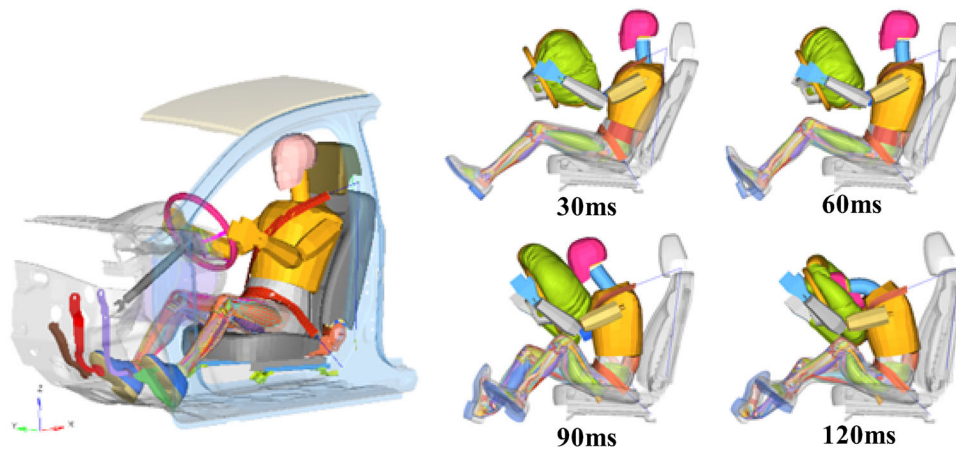


FIGURE 10. Offset crash simulation model and occupant kinematics during crash.

without it were implemented. The occupant model was set up by coupling the lower limb-pelvis model and a Hybrid III dummy upper body model at the pelvis center. The entire model and the driver’s kinematics during the whole impact were shown in Fig. 10.

A serious femur fracture appeared in the junction of the left femoral small rotor and femoral shaft. Several acetabular wall and edge fracture existed in acetabulum region, while patella fracture also occurred. Concerning the bending moment and axial force through the femur, both levels varied significantly when comparing the case with active muscle forces to the one without them (Fig. 11). At initial phase, the axial force was partly increased by active muscle force. However, the peak axial force when bone fracture occurred was decreased from 6.8 to 5.97 kN. On the other hand, the peak bending moment increased from 163.5 to 175.3 Nm. This also indicated that the femur fracture

can be attribute to the combination of both axial force and bending moment. The position of the maximum bending moment also showed a variance due to the introduction of active muscle forces.

### DISCUSSION AND CONCLUSION

This study presents the development, validation and application of a lower extremity-pelvis FE model with 3D active muscles. By the integration of some features of musculoskeletal models, the present model showed its availability to directly monitor injury parameters of anatomy tissues during the whole joint movement, like stress distribution, internal force and moment. This indicated that this type of model can better simulate *in vivo* tissue responses during various loading conditions compared with common lower limb finite element



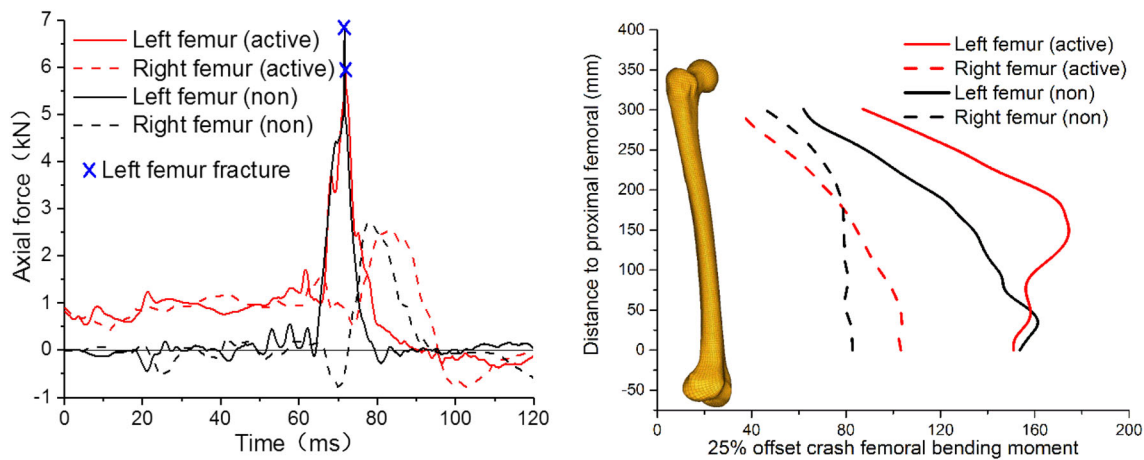


**FIGURE 11. Femoral axial forces and section bending moments.**

models with only passive properties. And it was also very valuable as a supplement to the PMHS or volunteer test to further understand injury mechanisms of the living tissues. Compared with the musculoskeletal model, the present active lower limb-pelvis FE was also partly limited due to the calculation time and stability when considering long time simulation.

Muscles of the model were represented using the combination of 1D truss and 3D solid elements. Passive properties of the muscles were mainly dependent on 3D solid elements. In the present study, QLV constitutive model and Ogden material model were respectively defined for 3D solid elements to simulate muscle passive properties with strain rate effects. Although QLV material show closer results to real responses in the experiments, it became unstable easily under both low and high strain rates. Regarding model stability and longer simulation time for medical application like gait analysis than safety analysis like car accident, Ogden material was finally selected for modeling passive properties of the muscles. For soft tissues especially the ones that are modeled with solid elements, the model accuracy and stability are generally needed to be balanced.

Bone tissues were modeled with both shell and solid elements. Especially for the epiphysis regions of long bones, different shell thickness and solid density were adopted according to detailed anatomy bone structure. As indicated by the Untaroiu *et al.* study,<sup>35</sup> the present study also found that this modeling method approximates better strain distribution and failure prediction in the epiphysis regions than the uniform thickness approach. In addition, bone tissues have been well investigated concerning its anisotropic and viscoelastic property from their microstructure to macro behavior in recent decades.<sup>7,10,12,27</sup> The present bone modeling

was still using isotropic materials regarding computing efficiency and stability of a global lower limb model. Although an elastic viscoplastic material model with continuous damage mechanics was used for spongy bone modeling in the present study, the detailed CDM parameters were not well determined according to our present validation related to the whole bone static and dynamic loading. Then the ultimate strain is dominant in damage prediction for both cortical and spongy bones. Due to hierarchical structure of the bone, its behavior under complex loading condition can be very complicated especially when concerning microscopic crack initiation and propagation. Thus, the improvement of the present model concerning bone materials and damage prediction should be implemented in the future.

In summary, the present model is the first step in developing an active lower limb-pelvis model for biomedical engineering and human safety analysis, and a useful tool to understand mechanisms of tissue injuries or related device design. The most advantage of this model is to monitor stress or strain variance of tissues in a dynamic simulation during walking or other activities. In this case, the loading environment of the model would be more realistic rather than quasi-static simulation of previous studies focusing on fixed joint status with specific definition of the boundary conditions.<sup>4,40</sup> With regard to the specific-subject features in biomedical application, the present model should be adjusted and further validated corresponding to research objectives. In addition, although the present model showed the availability to simulate active muscle contraction, further studies can be implemented to include muscular reflex and posture stability control for this type of active model.

## APPENDIX

See Table 3.

TABLE 3. Definition of muscle properties.

Muscles	PCSA (mm <sup>2</sup> )	F <sub>max</sub> (N)	Muscles	PCSA (mm <sup>2</sup> )	F <sub>max</sub> (N)
Satorious	312	156	Tibialis anterior	1810	905
Vastus rectus	2338	1169	Extensor digitorum longus	1024	512
Vastus intermedius	2730	1365	Extensor hallucis longus	324	162
Vastus lateralis	3742	1871	Peroneus longus	1886	943
Vastus medialis	2588	1294	Peroneus brevis	870	435
Gracilis femoris	324	162	Lateral head of gastrocnemius	1366	683
Adductor magnus	2424	1212	Medial head of gastrocnemius	3116	1558
Long head of biceps brachii	1792	896	Soleus	7098	3549
Short head of biceps brachii	1608	804	Tibialis posterior	3116	1558
Semitendinosus	820	410	Flexor digitorum longus	620	310
Semimembranous	2576	1288	Flexor hallucis longus	644	322

## ACKNOWLEDGMENTS

This work is supported by National Natural Science Foundation of China (Grant Nos. 51405150, 51475154) and Hunan Province Science and Technology Plan (Grant No. 2015JJ3052).

## REFERENCES

- <sup>1</sup>Anderson, A. E., C. L. Peters, B. D. Tuttle, and J. A. Weiss. Subject-specific finite element model of the pelvis: development, validation and sensitivity studies. *J. Biomech. Eng.* 127(3):364–373, 2005.
- <sup>2</sup>Arnold, E. M., S. R. Ward, R. L. Lieber, and S. L. Delp. A model of the lower limb for analysis of human movement. *Ann. Biomed. Eng.* 38(2):269–279, 2010.
- <sup>3</sup>Arnoux, P. J., D. Cesari, M. Behr, L. Thollon, and C. Brunet. Pedestrian lower limb injury criteria evaluation: a finite element approach. *Traffic Inj. Prev.* 6(3):288–297, 2005.
- <sup>4</sup>Bae, J. Y., K. S. Park, J. K. Seon, and I. Jeon. Analysis of the effects of normal walking on ankle joint contact characteristics after acute inversion ankle sprain. *Ann. Biomed. Eng.* 43(12):3015–3024, 2015.
- <sup>5</sup>Behr, M., P. J. Arnoux, T. Serre, L. Thollon, and C. Brunet. Tonic finite element model of the lower limb. *J. Biomech. Eng.-Trans. ASME.* 128(2):223–228, 2006.
- <sup>6</sup>Beillas, P., P. C. Begeman, K. H. Yang, *et al.* Lower limb: advanced FE model and new experimental data. *Stapp Car Crash J.* 2001(45):469–494, 2001.
- <sup>7</sup>Blanchard, R., A. Dejacco, E. Bongaers, and C. Hellmich. Intravoxel bone micromechanics for micro CT-based finite element simulations. *J. Biomech.* 46(15):2710–2721, 2013.
- <sup>8</sup>Cao, L., X. Du, G. Zhang, Y. Hu, and K. Zhang. Development and validation of the 50th percentile chinese male lower leg FE model. *Automot. Eng.* 37(11):1291–1297, 2015.
- <sup>9</sup>Crandall, J. Crashworthiness and Biomechanics, Euro-motor Course, June 11–13 2001.
- <sup>10</sup>Deseri, L., M. D. Paola, M. Zingales, and P. Pollaci. Power-law hereditariness of hierarchical fractal bones. *Int. J. Numer. Methods Biomed. Eng.* 29(12):1338–1360, 2013.
- <sup>11</sup>Hayashi, S., H. Y. Choi, R. S. Levine, K. H. Yang, A. I. King. Experimental and analytical study of knee fracture mechanisms in a frontal knee impact. 40th Stapp Car Crash Conference, Albuquerque, New Mexico, Paper No. 952729, 1996.
- <sup>12</sup>Hellmich, C., C. Kober, and B. Erdmann. Micromechanics-based conversion of CT data into anisotropic elasticity tensors, applied to FE simulations of a mandible. *Ann. Biomed. Eng.* 36(1):108–122, 2008.
- <sup>13</sup>Ivarsson, B. J., D. Genovese, J. R. Crandall, J. Bolton, C. Untaroiu, and D. Bose. The tolerance of the femoral shaft in combined axial compression and bending loading. *Stapp Car Crash J.* 53:251–290, 2009.
- <sup>14</sup>Iwamoto, M., A. Tamura, K. Furusu, C. Kato, K. Miki, J. Hasegawa, K. H. Yang. Development of a Finite Element Model of the Human Lower Extremity for Analyses of Automotive Crash Injuries SAE 2000 World Congress & Exhibition, Detroit, Michigan, USA, Paper No. 2000-01-0621, 2000.
- <sup>15</sup>Jammes, Yves, Michel Behr, Maxime Llari, Sarah Bonicel, J. P. Weber, and S. Berdah. Emergency braking is affected by the use of cruise control. *Traffic Inj. Prev.* 2017. doi: 10.1080/15389588.2016.1274978.
- <sup>16</sup>Jiang, X. Q. A Study on the Biomechanical of Occupant Lower Extremity Injuries in Car Frontal Impact Based on Human Body Model. PhD dissertation, Hunan University, 2014.
- <sup>17</sup>Kerrigan, J. R., K. S. Bhalla, N. J. Madeley, J. R. Funk, D. Bose, J. R. Crandall. Experiments for establishing pedestrian-impact lower limb injury criteria. SAE 2003 World Congress & Exhibition, Detroit, Michigan, USA, Paper No. 2003-01-0895, 2003a.
- <sup>18</sup>Kerrigan, J. R., D. C. Drinkwater, C. Y. Kam, *et al.* Tolerance of the human leg and thigh in dynamic latero-medial bending. *Int. J. Crashworth.* 9(6):607–623, 2004.

- <sup>19</sup>Kikuchi, Y., and Y. Takahashi. Development of a Finite Element Model for a Pedestrian Pelvis and Lower Limb. Detroit: SAE World Congress; 2006, 2006.
- <sup>20</sup>Kitagawa, Y., H. Ichikawa, A. I. King, R. S. Levine. A severe ankle and foot injury in frontal crashes and its mechanism. SAE 1998 World Congress & Exhibition, Detroit, Michigan, USA, Paper No. 983145, 1998.
- <sup>21</sup>Li, F., H. Li, W. Hu, S. Su, and B. Wang. Simulation of muscle activation with coupled nonlinear FE models. *J. Mech. Med. Biol.* 16(06):1650082, 2016.
- <sup>22</sup>Mo, F., P. J. Arnoux, D. Cesari, and C. Masson. Investigation of the injury threshold of knee ligaments by the parametric study of car-pedestrian impact conditions. *Saf. Sci.* 62:58–67, 2014.
- <sup>23</sup>Mo, F., C. Masson, D. Cesari, and P. J. Arnoux. Coupling lateral bending and shearing mechanisms to define knee injury criteria for pedestrian safety. *Traffic Inj Prev.* 14(4):378–386, 2013.
- <sup>24</sup>Myers, B. S., C. A. Van Ee, D. L. Camacho, C. T. Woolley, T. M. Best. On the structural and material properties of mammalian skeletal muscle and its relevance to human cervical impact dynamics. Stapp Car Crash Conference, Paper No. 0148-7191, 1995.
- <sup>25</sup>Myers, B. S., C. T. Woolley, T. L. Slotter, W. E. Garrett, T. M. Best, and W. Madison. The influence of strain rate on the passive and stimulated engineering stress-large strain behavior of the rabbit tibialis anterior muscle. *J. Biomech. Eng.* 120(1):126–132, 1998.
- <sup>26</sup>Neumann, D. A. Kinesiology of the Musculoskeletal System: Foundations for Physical Rehabilitation. St. Louis: Mosby/Elsevier, 2010.
- <sup>27</sup>Nguyen, L., S. Stoter, T. Baum, J. Kirschke, M. Ruess, Z. Yosibash, and D. Schillinger. Phase-field boundary conditions for the voxel finite cell method: surface-free stress analysis of CT-based bone structures. *Int J Numer Methods Biomed. Eng.* 2017. doi:10.1002/cnm.2880.
- <sup>28</sup>Rupp, J. D., M. P. Reed, C. A. Van Ee, S. Kuppa, S. C. Wang, J. A. Goulet, and L. W. Schneider. The tolerance of the human hip to dynamic knee loading. *Stapp Car Crash J.* 46(46):211–228, 2002.
- <sup>29</sup>Shigeta, K., Y. Kitagawa, T. Yasuki. Development of Next Generation Human FE Model Capable of Organ Injury Prediction. The 21st International Technical Conference on the Enhanced Safety of Vehicles Conference (ESV), Stuttgart, Germany, Paper No. 09-0111, 2009.
- <sup>30</sup>Shin, J., N. Yue, and C. D. Untaroiu. A finite element model of the foot and ankle for automotive impact applications. *Ann. Biomed. Eng.* 40(12):2519–2531, 2012.
- <sup>31</sup>Takahashi, Y., Y. Kikuchi, F. Mori, A. Konosu. Advanced FE Lower limb model for pedestrians. 18th International Technical Conference on the Enhanced Safety of Vehicles (ESV), Nagoya, Japan, Paper No. 218, 2003.
- <sup>32</sup>Thelen, D. G., and F. C. Anderson. Using computed muscle control to generate forward dynamic simulations of human walking from experimental data. *J Biomech.* 39(6): 1107–1115, 2006.
- <sup>33</sup>Untaroiu, C., K. Darvish, J. Crandall, B. Deng, and J. T. Wang. A finite element model of the lower limb for simulating pedestrian impacts. *Stapp Car Crash J.* 2005(49): 157–181, 2005.
- <sup>34</sup>Untaroiu, C., B. Ivarsson, D. Genovese, D. Bose, and J. Crandall. Biomechanical injury response of leg subjected to dynamic combined axial and bending loading. *Biomed. Sci. Instrum.* 44:141–146, 2008.
- <sup>35</sup>Untaroiu, C., N. Yue, and J. Shin. A finite element model of the lower limb for simulating automotive impacts. *Ann. Biomed. Eng.* 41:1–14, 2012.
- <sup>36</sup>Watanabe, R., H. Miyazaki, Y. Kitagawa, T. Yasuki. Research of Collision Speed Dependency of Pedestrian Head and Chest Injuries Using Human FE Model (THUMS Version 4). The 22nd International Technical Conference on the Enhanced Safety of Vehicles (ESV), Washington, D.C., Paper No. 11-0043, 2011.
- <sup>37</sup>Winters, J. M., and L. Stark. Analysis of fundamental human movement patterns through the use of in-depth antagonistic muscle models. *IEEE Trans. Biomed. Eng.* 10:826–839, 1985.
- <sup>38</sup>Winters, J. M., and L. Stark. Estimated mechanical properties of synergistic muscles involved in movements of a variety of human joints. *J Biomech.* 21(12):1027–1041, 1988.
- <sup>39</sup>Wittek, A., and J. Kajzer. Modeling of muscle influence on the kinematics of the head-neck complex in impacts. *Mem. School Eng. Nagoya University* 49:151–205, 1997.
- <sup>40</sup>Yao, J., C. Wen, T. Cheung, M. Zhang, Y. Hu, C. Yan, K. Y.-P. Chiu, et al. Deterioration of stress distribution due to tunnel creation in single-bundle and double-bundle anterior cruciate ligament reconstructions. *Ann. Biomed. Eng.* 40(7):1554–1567, 2012.